Electronic Supplementary Information for:

Cooperative Self-Assembly Driven by Multiple Noncovalent Interactions: Investigating Molecular Origin and Reassessing Characterization

Samaresh Samanta,[a] Parth Raval,[b] G. N. Manjunatha Reddy*[b] and Debangshu Chaudhuri*[a]

[a] *Department of Chemical Sciences, Indian Institute of Science Education and Research (IISER) Kolkata, Mohanpur 741246, India. Email: dchaudhuri@iiserkol.ac.in*

[b] *Univ. Lille, CNRS, Centrale Lille Institut, Univ. Artois, UMR 8181, Unité de Catalyse et Chimie du Solide, F-59000, Lille, France. Email: gnm.reddy@univ-lille.fr*

Table of contents

1. Materials and Methods

All chemicals and spectroscopy grade solvents were purchased from Sigma Aldrich Chemical Co. and used without further purification.

^{1}H and ^{13}C NMR spectroscopy in solution were performed on AVANCE III 500 Bruker spectrometer, and the data were calibrated against TMS.

Mass Spectroscopy (ESI-MS) data was acquired in positive mode electron spray ionization using the Bruker Maxis II^{TM} instrument.

Circular Dichroism Spectroscopy was carried out on JASCO J-815 CD spectrometer. Temperature and solvent composition dependent measurements were carried out following the same experimental parameters as in the case of absorption spectroscopy.

Optical absorption spectroscopy based experiments were performed on Cary 300 and Shimadzu UV 2600 spectrophotometer, fitted with S-1700 thermoelectric single cell holder to regulate sample temperature. For temperature dependent absorption spectroscopy experiments, a heating/cooling rate of 1 °C/min was used. In solvent composition dependent study, small aliquots of the good solvent ($CHCl_3$ or ^{t}BuOH) were added to a solution of **PBI-1** in methylcyclohexane, ensuring that the concentration of **PBI-1** remained strictly unchanged. After each addition, the solution was stirred for 1 minute to re-establish the equilibrium, and brought to rest before recording the spectrum. All optical spectroscopy-based experiments were carried out with dilute solutions (~10-25 μM).

Solid-state NMR spectroscopy. **PBI-1** aggregates in methylcyclohexane (MCH) tend to precipitate out over a few hours. The solid aggregate thus formed was separated by centrifugation, washed with fresh MCH, and dried under dynamic vacuum for solid state NMR spectroscopy. All the 1D ^{1}H and ^{13}C, and 2D ^{1}H-^{1}H and ^{1}H-^{13}C correlation NMR experiments on **PBI-1** were carried out on a Bruker Avance Neo (18.8T) spectrometer using either a 1.3 mm H-X or a 3.2 mm H-X probehead tuned to ^{1}H (Larmor frequency, 800.1 MHz) and ^{13}C (Larmor frequency, 201.2 MHz) nuclei. The nutation frequency for ^{1}H was 100 kHz, corresponding to 90° pulse duration of 2.5 μs and 94.3 kHz for ^{13}C corresponding to 90° pulse duration of 2.7 μs. All 1D and 2D fast MAS experiments were carried out at a MAS frequency of 56 kHz using a 1.3 mm H-X probe. The longitudinal relaxation time (T_1) of ^{1}H was determined to be 2.5 s based on inversion recovery measurements and analyses. 1D ^{1}H MAS NMR spectrum was acquired using 4 co-added transients. A 2D ^{1}H-^{1}H double-quantum (DQ)-single-quantum (SQ) NMR spectrum of **PBI-1** was acquired using Back-to-Back (BaBa) sequence.[1] The DQ coherences were excited and reconverted using a 16-step phase cycle to choose $\Delta p = \pm 2$ on the DQ excitation pulses (4 steps) and $\Delta p = \pm 1$ (4 steps), where p is the coherence order. A rotor-synchronized t_1 increment was applied with different recoupling times of 17.8 μs, 35.6 μs, and 71.2 μs, which correspond to one, two, and four rotor periods (τ_r).The indirect ^{1}H DQ dimension was acquired using 140 t_1 increments, each with 16 co-added transients, corresponding to a total experimental time of 1.2 h using a 2 s recycle delay. ^{1}H detected 2D ^{1}H-^{13}C heteronuclear correlation (HETCOR) spectra were acquired using 2, 3 and 4 ms of CP contact time and compared. Indirect ^{13}C dimension was acquired using 140 t_1 increments, each with 32 co-added transients, corresponding to a total experimental time of 2.5 h each, using a 2 s recycle delay. 2D ^{1}H-^{13}C HETCOR spectra were acquired using 50 kHz MAS.

Solvent-induced disassembly process was monitored using *ex-situ* ^{1}H MAS NMR experiments, by titrating **PBI-1** powder with different weight fractions of chloroform-d and ethanol-d6. For a titration experiment

with ethanol, vials containing 5 mg of **PBI-1** powder were treated with 2, 4, 6, and 8 µl of solvent that correspond to **PBI-1**:EtOD, wt/wt, 74:26, 58:42, 48:52, and 41:59, respectively. The slurry-like samples containing different **PBI-1**:EtOD, wt/wt, ratio were packed into 3.2 mm high-resolution magic-angle spinning (HR-MAS) zirconia rotors and fitted with inserts/sealing-screws and Kel-F® caps in order to avoid leakage of solvent during MAS experiments. *Ex-situ* ^{1}H MAS NMR experiments were carried out for these samples at variable spinning speed (8-20 kHz MAS) and compared with 1D ^{1}H NMR of 5 mg of neat **PBI-1** acquired under the same conditions except at 20 kHz MAS. Likewise, for a titration with chloroform-d, vials containing 5 mg of **PBI-1** were titrated with 2, 6, and 12 µl of $CDCl_3$ leading slurry-like samples of **PBI-1**:$CDCl_3$, wt/wt, 63:37, 35:65 and 22:78, respectively. All 1D ^{1}H MAS experiments were acquired with 64 co-added transients and a recycling delay of 3 s, resulting in a total experimental time of 3.2 minutes each. ^{1}H and ^{13}C chemical shifts were calibrated to TMS using adamantane as an external reference at 1.8 ppm and 38.4 ppm (high-frequency signal), respectively, for all the experiments.

SAFETY STATEMENT: No unexpected or unusually high safety hazards were encountered.

2. Synthesis and Characterization

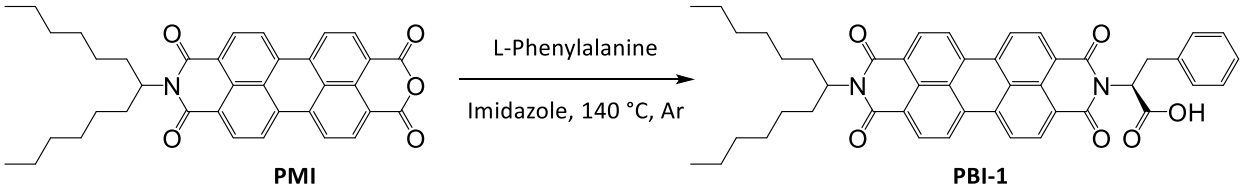

PMI **PBI-1**

Perylene monoimide (PMI) was prepared following a reported procedure.[2] In a 250 ml round bottom flask PMI (0.4 g, 0.69 mmol), L-Phenylalanine (0.114 g, 0.69mol), and imidazole (5.0 g) was stirred under argon at 140°C for 8 h. The reaction mixture was cooled to 100°C, and 50 ml ethanol was added to it. The reaction mixture was further cooled to room temperature, and 150 ml 2N HCl was poured. The precipitate was collected through filtration, washed with hexane, and the crude product was purified by silica gel column chromatography using $CHCl_3$/MeOH (3%) as eluent to produce 0.25 g (34 % yield) of **PBI-1** as red solid. ^{1}H NMR ($CDCl_3$, 500 MHz) 8.62-8.40 (m, 8H); 7.24-7.23 (d, 1H); 7.16-7.13 (t, 2H); 7.09-7.06 (t, 1H); 6.16-6.13 (q, 1H) 5.18 (q, 1H); 3.77-3.73 (dd, 1H); 3.59-3.54 (dd, 1H); 2.27-2.22 (m, 2H); 1.90-1.84 (m, 2H); 1.36-1.23 (m, :γCH2, 16H), 0.84-0.81 (t, CH_3, 6H); ^{13}C NMR ($CDCl_3$, 125 MHz): 173.6, 162.78, 137.01, 134.09, 134.01, 131.70, 129.98, 129.24, 128.37, 126.68, 126.27, 126.15, 123.20, 122.85, 122.30, 54.09, 54.84, 34.91, 32.62, 31.84, 29.51, 26.93, 22.56, 14.02. MS (ESI-MS): m/z calculated for $[M]^{2+}$ 360.425, found 360.325; calculated for $[M\text{-}Na]^{+}$ 743.84, found 743.31.

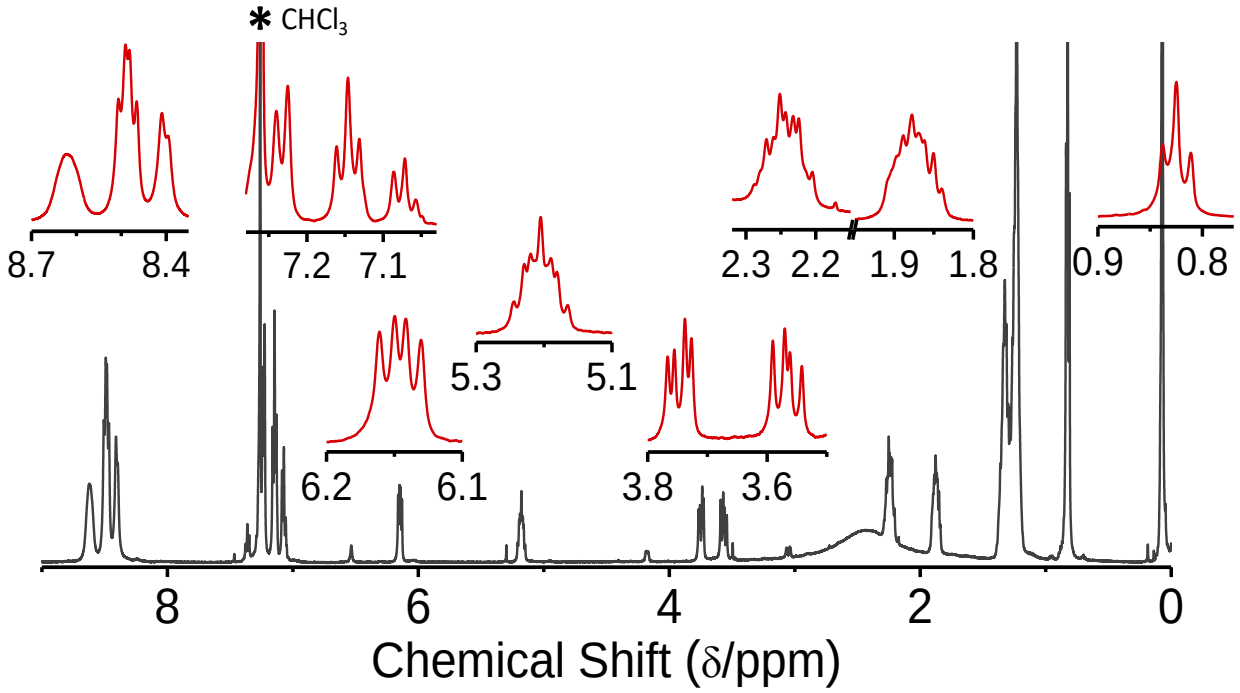

Figure S1. ^{1}H NMR (500 MHz, $CDCl_3$, 298K) spectrum of **PBI-1**. The insets present a magnified view of specific ^{1}H resonances.

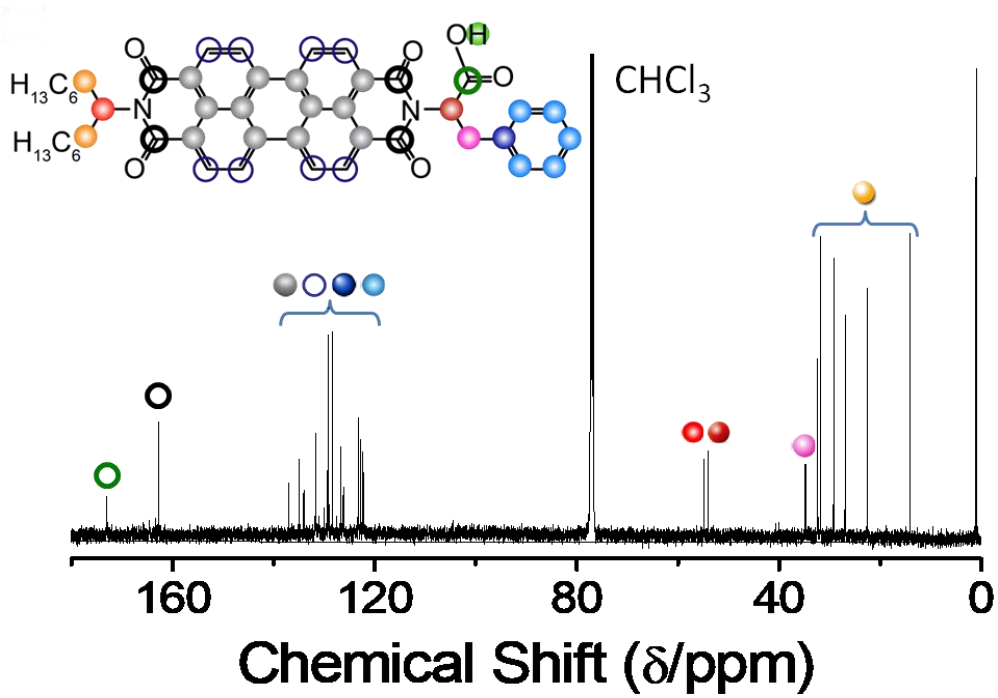

Figure S2. ^{13}C NMR (125 MHz, $CDCl_3$, 298K) of **PBI-1**.

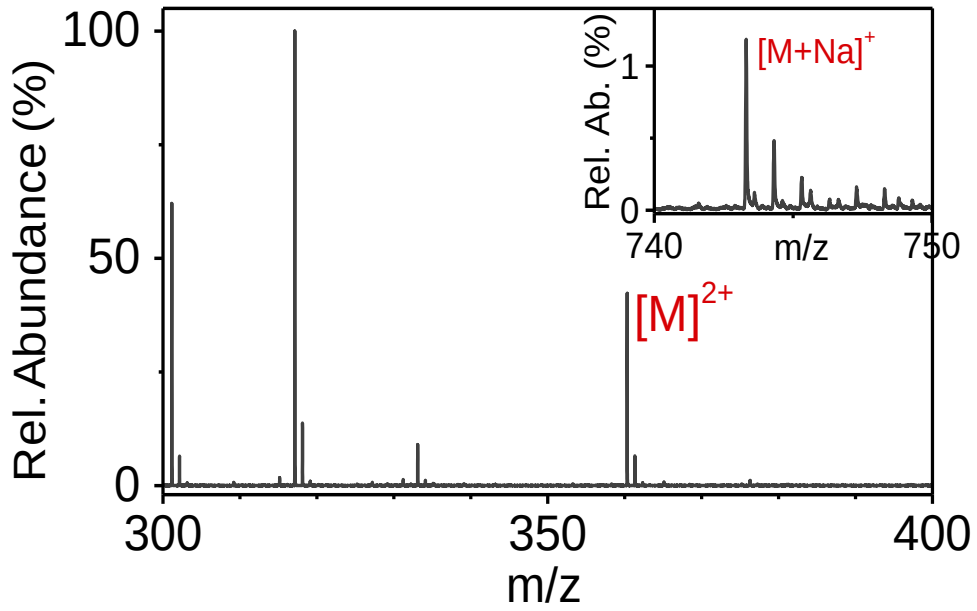

Figure S3. ESI-Mass spectrum of **PBI-1**.

3. Analysis of temperature dependent α_{Agg}

Temperature dependent degree of aggregation (α_{Agg}) was calculated from the $A_{0\text{-}0}$ (at 515 nm), using the formula,

$$\alpha_{\mathrm{Agg}}(T) = \frac{A_{0-0}(375\ \mathrm{K}) - A_{0-0}(T)}{A_{0-0}(375\ \mathrm{K}) - A_{0-0}(298\ \mathrm{K})} \qquad (1)$$

The analysis of $\alpha_{\mathrm{Agg}}(T)$ was done using the mass balance model and the program developed by ten Eikelder and coworkers.[3] The model describes the cooperative growth of one-dimensional aggregates of a molecule *M* by assuming a dimeric nucleus. The two equilibrium steps are therefore:

$$\text{Nucleation:} \quad M + M \rightleftharpoons M_2$$

$$\text{and Elongation:} \quad M_l + M \rightleftharpoons M_{l+1}\ ;\ l \geq 2$$

The equilibrium constants for the two processes are given by K_n and K_{el}, and the degree of cooperativity is defined as $\sigma = K_n/K_{el}$.

Principle of detailed balance allows one to express the concentration of aggregates of different lengths (l) in terms of the free monomer concentration (C_{mon}). Taking into account aggregates of all possible lengths ($2 \leq l \leq \infty$), the monomer concentration in the aggregated form is expressed as:

$$C_{Agg} = \sigma C_{mon} \sum_{l=2}^{\infty} l(K_{el}C_{mon})^{l-1}$$

$$= \sigma C_{mon} \frac{K_{el}C_{mon}(2 - K_{el}C_{mon})}{(1 - K_{el}C_{mon})^2} = \frac{\sigma K_{el}C_{mon}^2\ (2 - K_{el}C_{mon})}{(1 - K_{el}C_{mon})^2} \qquad (2)$$

The total monomer concentration in solution is given by, $C_{tot} = C_{mon} + C_{Agg}$, and the degree of aggregation as: $\alpha_{\mathrm{Agg}} = C_{Agg}/C_{tot}$

Within this model, the effect of temperature on α_{Agg} is included through the temperature dependence of K_{el} and σ, described as:

$$K_{el} = \exp\left(-\frac{\Delta G^{\circ}_{el}}{RT}\right);\ \Delta G^{\circ}_{el} = \Delta H^{\circ}_{el} - T\Delta S^{\circ}_{el} \qquad (3)$$

$$K_n = \exp\left(-\frac{\Delta G^{\circ}_{n}}{RT}\right);\ \Delta G^{\circ}_{n} = \Delta H^{\circ}_{n} - T\Delta S^{\circ}_{n} = \Delta H^{\circ}_{el} - \Delta H^{\circ}_{NP} - T\Delta S^{\circ}_{n}, \qquad (4)$$

where ΔH°_{NP} is the nucleation penalty. Assuming $\Delta S^{\circ}_{el} = \Delta S^{\circ}_{n}$, one can write:

$$\sigma = \frac{K_n}{K_{el}} = \exp\left(\frac{\Delta H^{\circ}_{NP}}{RT}\right) \qquad (5)$$

Simulating temperature dependence of α_{Agg} is done by solving the equation $C_{tot} = C_{mon} + C_{Agg}$ for C_{mon} at different temperatures, using parameters $\Delta H^{\circ}_{el}, \Delta H^{\circ}_{NP}$ and ΔS°_{n} and experimentally known C_{tot}.

Table S1. Thermodynamic parameters obtained from the analysis of temperature dependent α_{Agg} from optical absorption spectroscopy.

C_{tot} (μM)	Best fit parameters					
	ΔH°_{el} (kJ/mol)	ΔS° (kJ/mol.K)	ΔH°_{NP} (kJ/mol)	T_e (K)	**ΔG°_{el} (kJ/mol) at 293 K**	**σ (at 293 K)**
15	−72.4 ± 0.97	−0.107± 0.003	−17.96 ± 0.53	362.7 ± 0.19	**−40.98** ± 0.41	**6.3×10^{4}**

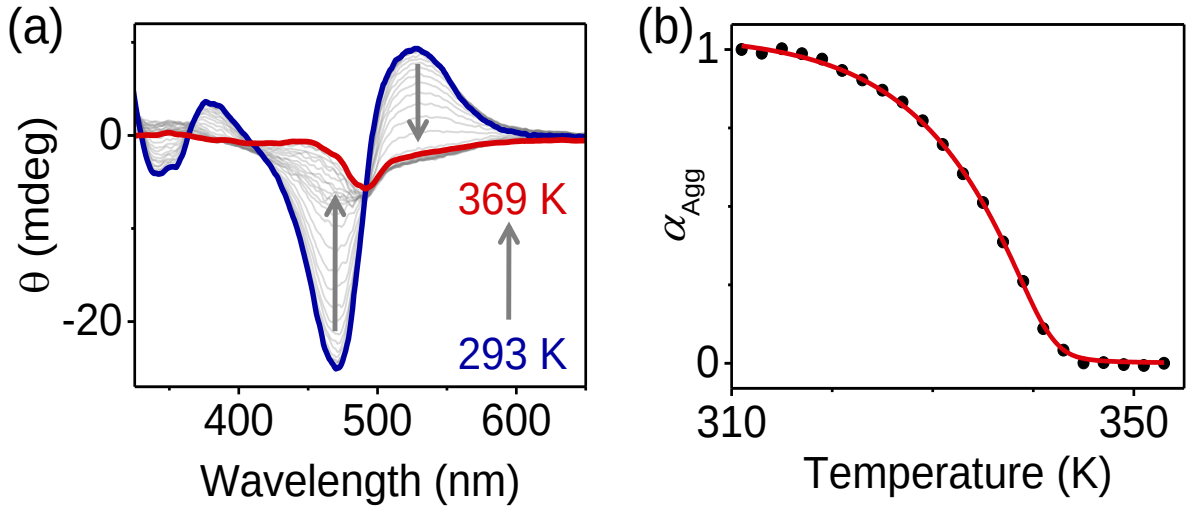

Figure S4. (a) Temperature dependent CD spectra of **PBI-1** aggregates in MCH (b) Variation of α_{Agg}, derived from ellipticity values (θ) at 529 nm. Red line shows the simulated curve generated using mass-balance model for $\sigma = 6.06\times10^{-4}$ and $\Delta G_{el} = -36.7 \pm 1.82$ kJ/mol, at 293 K.

4. DFT calculations

All the DFT calculations were performed using Gaussian 16 package.[4] The structure of an isolated **PBI-1** molecule was optimized to a ground-state equilibrium geometry using the B3LYP functional and aug-cc-pvdz basis set. The optimized structure of **PBI-1** was then used to calculate NMR shieldings using the gauge-independent atomic orbital (GIAO) method, the B3LYP/6-31G functional and basis set. DFT-calculated ^{1}H and ^{13}C chemical shifts were referenced to the ^{1}H shifts of TMS calculated using the B3LYP/6-311+G(2d,p) functional (included in the Gaussian 16 package). DFT-calculated ^{13}C chemical shifts were plotted against experimental ^{13}C chemical shifts, as shown in Figure S5. A regression analysis was carried out by constraining the slope to 1.0.[5] This analysis leads to a linear correlation between the experimental and DFT calculated ^{13}C chemical shifts with an intercept of 7.1, meaning that 7.1 ppm needs to be added to DFT calculated chemical shifts in order to compare with the experimental ^{13}C chemical shifts.

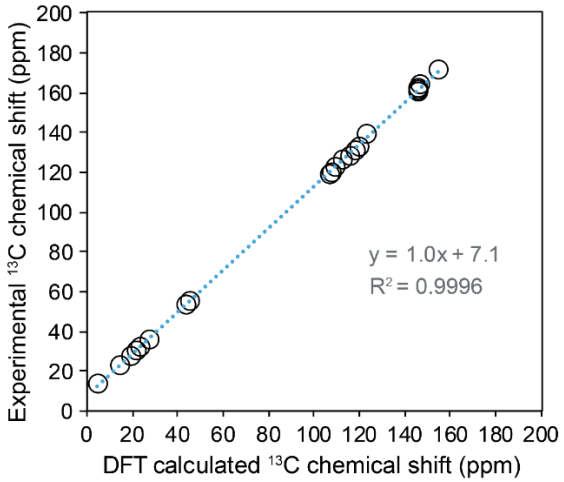

Figure S5. Experimental ^{13}C chemical shifts are plotted against DFT calculated ^{13}C chemical shifts.

5. Analysis of ^{1}H→^{13}C CP signal intensity buildup

In a ^{13}C{^{1}H} cross-polarization (CP) MAS NMR experiment,^{1}H and ^{13}C nuclei are simultaneously excited in order to enhance the ^{13}C signal intensities via ^{1}H→^{13}C spin polarization. The CP transfer is mediated by the dipole-dipole interactions between ^{1}H and X spins (here, X = ^{13}C). At lower CP contact times of ≤0.1 ms, the ^{13}C signals of direct covalently bonded C-H moieties are enhanced. At longer (>0.1 ms) CP contact times, the polarization transfer takes place between the heteronuclear C-H spins that are further apart, i.e., via through-space inter- and intramolecular C-H proximities up to 10 Å, leading to the enhancement of ^{13}C signals corresponding to both directly bonded C-H moieties as well as tertiary carbon atoms. The C-H proximities can be estimated by analyzing ^{1}H→^{13}C CP signal intensity buildup as a function of CP contact times. We carried out ^{13}C CP-MAS NMR experiments on solid **PBI-1** aggregates as a function of CP contact time (Figure S6a) in order to understand CP signal intensity buildup. Analyses of ^{13}C CP signal intensity buildup curves (Figure S6b,c) reveal that both aliphatic and aromatic C-H moieties exhibit maximal ^{13}C signal enhancements in the range of 4-7 ms of CP contact time.

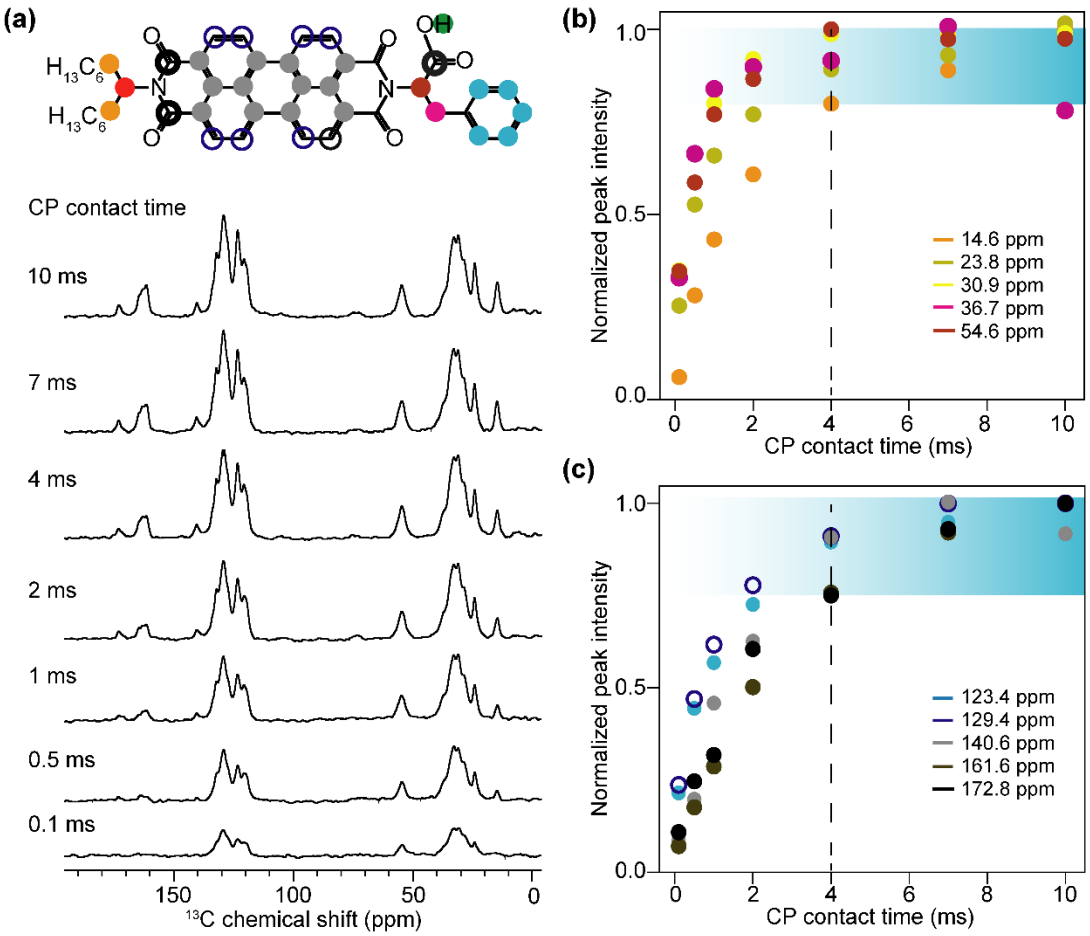

Figure S6. (a) 1D ^{13}C CP-MAS NMR spectra of **PBI-1** acquired at 15 kHz MAS using different CP contact times depicted alongside each spectrum. Plots of $^{1}H \rightarrow ^{13}C$ CP signal intensity buildup as a function of CP contact time of (b) aliphatic and (c) aromatic ^{13}C signals. Color codes of buildup curves correspond to the color codes depicted in the inset structure schematic. For both aliphatic and aromatic C-H moieties, enhanced CP intensity buildup is obtained for the CP contact time of over 4 ms.

6. 2D ^{1}H-^{13}C heteronuclear correlation (HETCOR) NMR spectrum of PBI-1

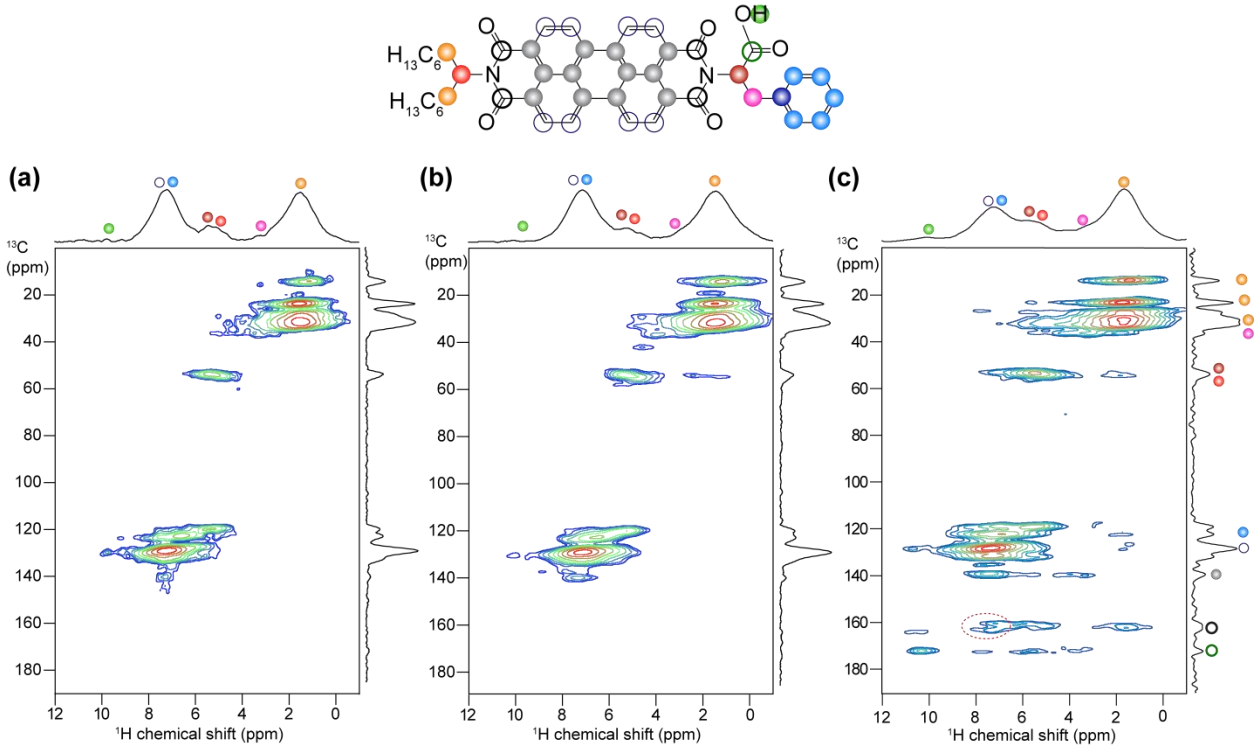

Figure S7. 2D ^{1}H-^{13}C heteronuclear correlation (HETCOR) spectra of **PBI-1** acquired at 18.8 T (^{1}H = 800.1 MHz and ^{13}C = 201.2 MHz) with 50 kHz MAS with (a) 2 ms, (b) 3 ms, and (c) 4 ms of CP contact times. Dashed oval indicates the 2D peak originating from the inter and intramolecular interactions in **PBI-1** aggregates.

Figure S7 compares 2D ^{1}H-^{13}C heteronuclear correlation spectra of **PBI-1** acquired with 2, 3, and 4 ms of CP contact times. In all 2D ^{1}H-^{13}C HETCOR spectra, the strong intensity 2D correlation peaks at 14.6, 23.8, and 32.1 ppm in the ^{13}C dimension and 1.4, 1.7, and 1.8 ppm in the ^{1}H dimension arise from directly bonded C-H moieties in the branched aliphatic sidechain of **PBI-1**. Detection of these C-H correlation signals is straightforward as they correspond to chemically distinct C-H moieties in CH_2 and CH_3 groups and proximities between them. The 2D correlation peak at 54.4 ppm in the ^{13}C dimension and 5.5 ppm in the ^{1}H dimension is ascribed to C_α-H carbon-proton pairs (red and burgundy dots). In the aromatic region, the intense correlation signals involving ^{13}C peaks at 119.6 and 123 ppm (^{13}C) with 7.0 (^{1}H) ppm arise due to covalently bonded C–H groups of the phenyl (Phe) ring. Similarly, one can identify 2D correlation peaks that correspond to the bonded C–H pairs of the perylene core at 128.6(^{13}C) × 7.4 ppm (^{1}H). In contrast, the 2D correlation between 119.6 ppm (^{13}C) and 5.5 ppm (^{1}H) suggests intramolecular ^{1}H···^{13}C dipolar coupling between aromatic C of the Phe (blue dots) and ^{1}H–C_α (burgundy dot). 2D peaks at 140.1 ppm (^{13}C) and 7.2, 5.5, 2.9 ppm (^{1}H) indicate intramolecular proximity of the tertiary aromatic C of the Phe (dark blue) to phenyl ring protons (blue dots), ^{1}H–C_α (burgundy) and benzylic protons (magenta), respectively. Intramolecular ^{1}H···^{13}C dipolar coupling between perylene tertiary carbons (grey dots) and perylene aromatic protons (blue circles) accounts for the peak at 136.2 ppm (^{13}C) and 7.4 ppm (^{1}H). The perylene carbons (blue open circles) (128.6 ppm) show the correlation

with perylene protons (7.4 ppm) and carboxylic proton (10.3 ppm). The four imide carbonyl carbons also exhibit through-space intramolecular coupling with a variety of protons. 2D correlation peaks at 161.6 ppm (^{13}C) and 1.6, 5.3, 7.2ppm (^{1}H) indicate that the imide carbonyl C (black circle) on the alkyl side is in close proximity to alkyl chain protons, ^{1}H-C$_{\alpha}$ (red dot) and phenyl protons (intermolecular), respectively. Likewise, the imide carbonyl C on the Phe side (164.8 ppm) interacts with the carboxylic acid proton at 10.3 ppm to result in a 2D correlation peak. 2D correlation peaks at 172.8 ppm (^{13}C) and 3.4, 5.8, 10.3 ppm (^{1}H) originate from an intramolecular dipolar interactions involving the carboxylic acid carbon and the benzylic protons (magenta), ^{1}H-C$_{\alpha}$ on the Phe side (burgundy) and acidic proton (green). Correlation peaks corresponding to remote ^{1}H-^{13}C pairs (i.e., weak dipolar interactions between ^{13}C and ^{1}H sites that are far with respect to each other) are not observed in the 2D ^{1}H-^{13}C spectra acquired with 2 and 3 ms CP contact times, as these contact times are not suitable to transfer the ^{1}H polarization to carbonyl groups with detectable signal intensities but are detected at 4 ms CP contact time (Figure S6).

Table S2. 2D ^{1}H-^{13}C correlation peaks observed in HETCOR NMR spectra of **PBI-1** aggregates acquired with different CP contact times.

^{1}H-^{13}C proximities	^{1}H chemical shift (ppm)	^{13}C chemical shift (ppm)	Observed in 2D HETCOR		
			2ms	3 ms	4 ms
Alkyl-Alkyl (terminal)	1.4	14.6	Yes	Yes	Yes
Alkyl-Alkyl (central)	1.7	23.8	Yes	Yes	Yes
Alkyl-Alkyl	1.8	32.1	Yes	Yes	Yes
C$_{\alpha}$-Alkyl	5.5	32.3	Yes	Yes	Yes
Alkyl-C$_{\alpha}$	1.9	54.4	No	Yes	Yes
C$_{\alpha}$-C$_{\alpha}$	5.5	54.4	Yes	Yes	Yes
Benzylic-Phenyl	2.9	119.6	No	No	Yes
C$_{\alpha}$-Phenyl	5.5	119.6	Yes	Yes	Yes
Phenyl-Phenyl	7.0	123.0	Yes	Yes	Yes
Alkyl-Phenyl	1.7	123.4	No	No	Yes
Alkyl-Perylene	1.6	128.4	No	No	Yes
Perylene-Perylene	7.4	129.4	Yes	Yes	Yes
Carboxylic-Perylene	10.3	129.4	Yes	Yes	Yes
Benzylic-Perylene	4.2	132.0	No	No	Yes
Perylene-Perylene(4^{O})	7.4	140.1	Yes	Yes	Yes
C$_{\alpha}$- Perylene(4^{O})	5.5	140.1	No	No	Yes
Benzylic- Perylene(4^{O})	3.4	140.1	No	No	Yes
Alkyl-Carbonyl[a]	1.6	161.6	No	No	Yes
C$_{\alpha}$-Carbonyl[a]	5.3	161.6	No	No	Yes
Phenyl-Carbonyl[a]	7.1	161.6	No	No	Yes
Perylene-Carbonyl[b]	7.4	164.8	No	No	Yes
Carboxylic acid-Carbonyl[b]	10.3	164.8	No	No	Yes
Benzylic-Carboxylic acid	3.4	172.8	No	No	Yes
C$_{a}$-Carboxylic acid	5.8	172.8	No	No	Yes
Perylene-carboxylic acid	7.8	172.8	No	No	Yes
Carboxylic acid-Carboxylic acid	10.4	172.8	No	No	Yes

[a] Carbonyl groups proximate to the alkyl sidechain

[b] Carbonyl groups proximate to the phenyl ring

7. 2D ^{1}H-^{1}H DQ-SQ correlation NMR spectrum of PBI-1

In a 2D ^{1}H DQ-SQ NMR experiment, correlation peaks corresponding to dipole-dipole coupled ^{1}H-^{1}H pairs in close proximities (<5 Å) can be detected and compared. Since ^{1}H-^{1}H dipolar interactions are partially averaged in a typical MAS experiment, a reintroduction of ^{1}H-^{1}H dipolar interactions needs to be achieved, for example, using a rotor synchronized recoupling sequence. To probe H-H proximities, 2D ^{1}H DQ-SQ NMR spectra were acquired with different recoupling times(i.e., the time allowed to reintroduce the dipolar interactions between ^{1}H-^{1}H spin pairs). The signal observed at a particular recoupling time is characteristic of the dipole-dipole coupling between H-H proximities and orientations. For instance, the spin pair that are spatially close to each other can be revealed with a very short recoupling time (τ_r), whereas the spin pair that are more distant are expected to be observed for a comparatively longer recoupling time ($4\tau_r$). In order to differentiate the ^{1}H-^{1}H proximities in **PBI-1**, we acquired ^{1}H-^{1}H DQ-SQ correlation NMR spectrum of **PBI-1** with one rotor period (17.8 μs) and four rotor period (71.2 μs) recoupling time, as shown in Figure S8.

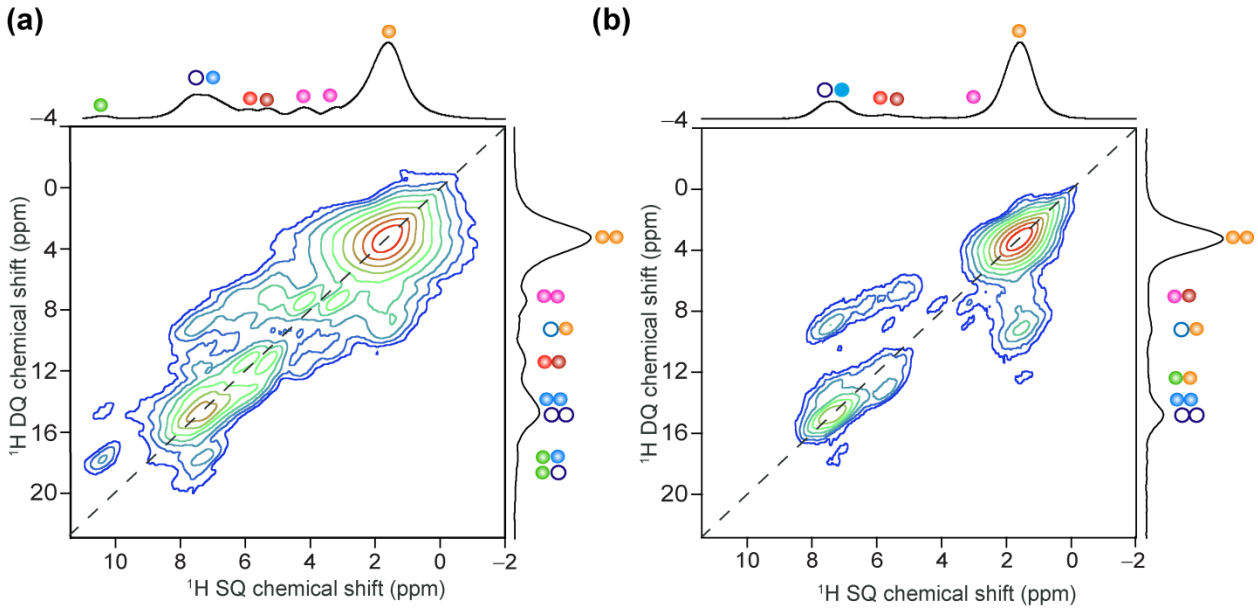

Figure S8. Solid-state 2D ^{1}H-^{1}H DQ-SQ correlation NMR spectra of **PBI-1** aggregates acquired at18.8 T (^{1}H, 800.1 MHz) and 56 kHz MAS using (a) 17.8 μs and (b) 71.2μs recoupling time, corresponding to $1\tau_r$ and $4\tau_r$, respectively.

In the 2D ^{1}H-^{1}H DQ-SQ correlation spectrum acquired with a recoupling time of 17.8 μs (i.e., $1\tau_r$), relatively fast DQ signal intensity buildup is observed for H-H pairs in close proximities such as CH_2 groups. As expected, the spectrum is dominated by two intense and broad autocorrelation signals centered at δ_{DQ} of 1.6 + 1.6 = 3.2 ppm and at 7.4 + 7.4 = 14.8 ppm. The former results from multiple through-space coupling within the alkyl chain, and the latter from aromatic protons. The off-diagonal DQ peak at 3.2 + 4.2 = 7.4 ppm is due to intramolecular ^{1}H···^{1}H proximity between the chemically inequivalent benzylic protons of Phe. By contrast, the H-H pairs that are spatially far with respect to each other (> 3Å) exhibit slower intensity buildup, leading to low-intensity ^{1}H DQ signals. For example, partially resolved ^{1}H DQ signals at 7.0, 7.7, and 9.0 ppm are attributed to the proximities between benzylic protons and alkyl sidechain protons, and aromatic protons and alkyl protons. The DQ peak at 7.4 + 10.3 = 17.7 ppm arises from dipole-dipole intermolecular interactions between carboxylic proton

and aromatic proton, further corroborating the formation of antiparallel stacking of **PBI-1**. In the 2D ^{1}H-^{1}H DQ-SQ correlation spectrum acquired with a recoupling time of 71.2 μs (i.e., $4\tau_r$), the intense ^{1}H DQ signals associated with distant H-H pairs are evolved, and simultaneously the ^{1}H DQ signal intensities of closely proximate H-H pairs are reduced, enabling the DQ signals at 7.0, 7.7 and 9.0 ppm corresponding to aromatic protons and alkyl sidechain protons to be resolved (Figure S8b).

Table S3. Experimental ^{1}H SQ and DQ chemical shifts of **PBI-1**

Proton site	^{1}H SQ chemical shift (ppm)	^{1}H DQ chemical shift (ppm)
Alkyl[a] + Alkyl[a]	1.6 + 1.6	3.2
Alkyl + C_α	1.7 + 5.3	7.0
-CH_2 + -CH_2	3.2 + 4.2	7.4
Alkyl + C_α	1.7 + 6.0	7.7
Alkyl[a] + Aromatic	1.6 + 7.4	9.0
C_α-C_α	5.3+6.0	11.3
-CH_2 + Aromatic	4.2 + 7.4	11.6
-CH_2 + Carboxylic	4.2 + 10.3	14.5
Aromatic + Aromatic	7.4 + 7.4	14.8
Aromatic + Carboxylic	7.4 + 10.3	17.7
Carboxylic + Carboxylic	10.3 + 10.3	20.6

[a] terminal or central alkyl proton

8. Analysis of solvent composition dependent α_{Agg}

$\alpha_{Agg}(f)$ was calculated from $A_{0\text{-}0}$ (at 515 nm), using the formula,

$$\alpha_{\mathrm{Agg}}(f) = \frac{A_{0-0}(f_{max}) - A_{0-0}(f)}{A_{0-0}(f_{max}) - A_{0-0}(f=0)} \qquad (1)$$

where f_{max} refers to the volume fraction of good solvent at which complete disassembly is achieved, and the absorption spectrum resembles that of molecularly dissolved **PBI-1**.

Analyses of $\alpha_{Agg}(f)$ were done using the model proposed by de Greef, Meijer, and coworkers.[6] The model starts with a very similar description of the cooperative process as described earlier, in terms of nucleation followed by elongation stage with distinct equilibrium constants, $K_n << K_{el}$ and $\sigma = K_n/K_{el}$. Assuming a dimeric (n=2) nucleus, the dimensionless mass balance equation can be written as:

$$x_{tot} = \sigma^{-1} \sum_{i=1}^{2} i(\sigma x)^i + \sigma \sum_{i=3}^{\infty} i x^i \qquad (2)$$

In the above equation, $x_{tot} = K_{el} C_{tot}$ and $x = K_{el} C_{mon}$ represent the dimensionless concentration of total and free monomer, respectively. The first term in Eq. 2 accounts for the monomer concentration in the form of species smaller than or equal to the nucleus, which in the current model is the free monomer and the dimeric nucleus. The second term accounts for all larger aggregated species.

Making use of infinite binomial series, Eq. 2 can be rewritten as:

$$x_{tot} = x + 2\sigma x^2 - \frac{\sigma x^3(2x-3)}{(x-1)^2} \qquad (3)$$

As the volume fraction of good solvent (f) is changed, the relative concentration of aggregated to monomeric species also changes. This is captured through the dependence of K_{el} on f, as per the following equation:

$$\Delta G^{\circ\prime} = \Delta G^{\circ} + mf = RT \ln K_{el} \qquad (4)$$

The free energy change of monomer association ($\Delta G^{\circ\prime}$) is assumed to be linearly dependent on f, and the quantity m provides a measure of how "good" a solvent is.

Simulation of experimental α_{Agg} vs. f curves was carried out in Origin v2016. A uniform grid for $x = K_{el}C_{mon}$ was chosen, such that $0 \leq x \leq 1$. Corresponding values for $x_{tot} = K_{el}C_{tot}$ and K_{el} were calculated using Eq. 3 for a chosen value of σ. Using x and x_{tot}, we evaluated $\alpha_{Agg} = (x_{tot} - x)/x_{tot}$. Further using Eq. 4, we obtained f from K_{el}, for a given C_{tot} and chosen values of ΔG° and m. The best agreement between these simulated α_{Agg} vs. f plots and the experimental data for each **PBI-1** concentration (C_{tot}) was obtained by optimizing three parameters: σ, ΔG° and m.

Table S4. Best-fit parameters for solvent composition dependence of α_{Agg} from optical absorption spectroscopy.

^{t}BuOH induced disassembly			
C_{tot} (μM)	**ΔG°_{el} (kJ/mol) at 293 K**	**m (kJ/mol)**	**σ**
24	-29	220	1
13.5	-29	270	1
9	-26	280	1
$CHCl_3$ induced disassembly			
20	-36.7	58	1
10	-36.7	58	1

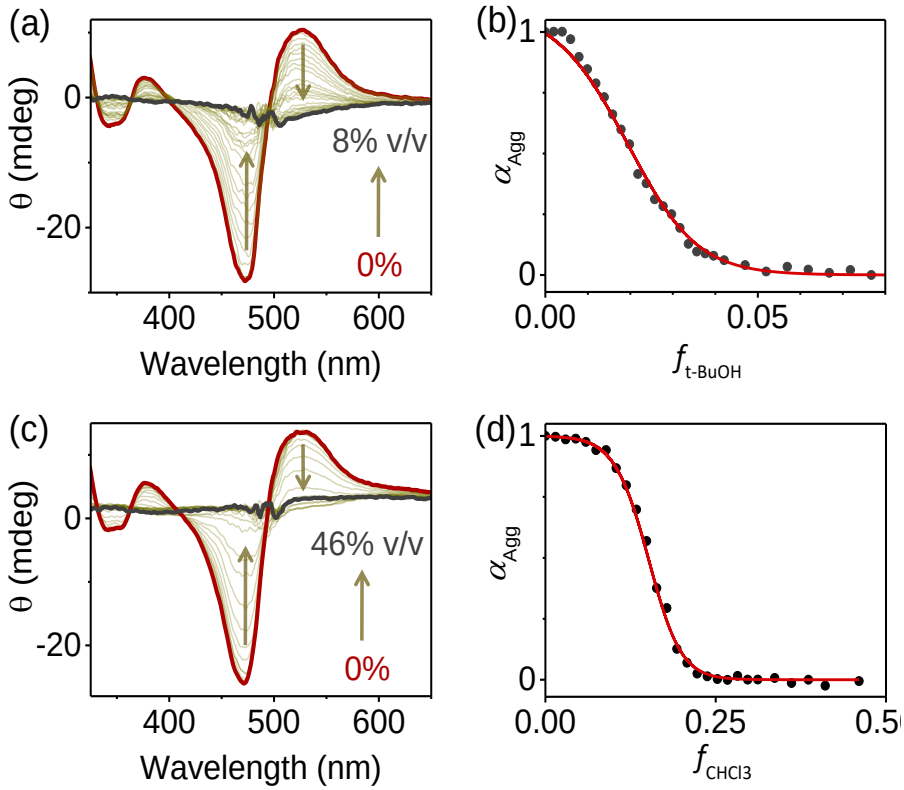

Figure S9. Solvent induced disassembly of **PBI-1** aggregates in MCH monitored by CD spectroscopy, using (a) ^{t}BuOH, and (c) $CHCl_3$ as good solvents. Corresponding α_{Agg} vs f plots can be fitted to the isodesmic model: (b) ΔG_{el} (293 K) = −27 kJ/mol, m = 320 kJ/mol (d) ΔG_{el} (293 K) = −37.5 kJ/mol, m = 110 kJ/mol.

9. Fast spinning limit for 1D ^{1}H MAS NMR spectrum of PBI-1

In molecular solids, anisotropic spin interactions such as chemical shift anisotropy and dipole-dipole couplings lead to line broadening in their NMR spectra. Magic-angle spinning (MAS, i.e., a spinning rotor containing solid sample inclined at an angle 54.7° with respect to the static magnetic field, B_0) technique allows to partially or completely average out these anisotropic interactions. Consequently, line narrowing is observed as a function of increased MAS frequency, facilitating enhanced spectral resolution and sensitivity at relatively higher MAS rates. In the case of **PBI-1**, the spectrum acquired with 20 kHz MAS shows well-resolved signals corresponding to different functional groups than the same spectrum recorded identical conditions except with 12.5 kHz MAS. However, subtle improvement in the spectral resolution was observed upon increasing MAS frequency from 20 kHz to 30 kHz and beyond (Figure S10), suggesting that the fast MAS limit associated with **PBI-1** is ~20 kHz. Furthermore, the addition of solvent leads to semi-solid aggregates, resulting in an improved resolution in the MAS NMR spectra at moderate spinning speeds (5-15 kHz MAS). The signal broadening at MAS rates of 10-12 kHz compared to 4 kHz MAS is expected to originate from the sedimentation or large domain aggregation caused by the mechanical force (centrifugal force) experienced by the sample inside the rotor. This line broadening and narrowing as a function of MAS rates in the range of 4-12 kHz is reversible. We

reasoned that the broader signals upon increasing MAS to 10-12 kHz are due to the PBI-1 solid aggregates that are deposited on the inner walls of the rotor (as seen in conventional centrifugation techniques), and the solution-like PBI-1 aggregates are locating at the central part of the cylindrical rotor whereby the sample experiences relatively lower mechanical force. At lower MAS rates of 4 kHz or below, the PBI-1 aggregates resemble a "slurry-like" mixture.

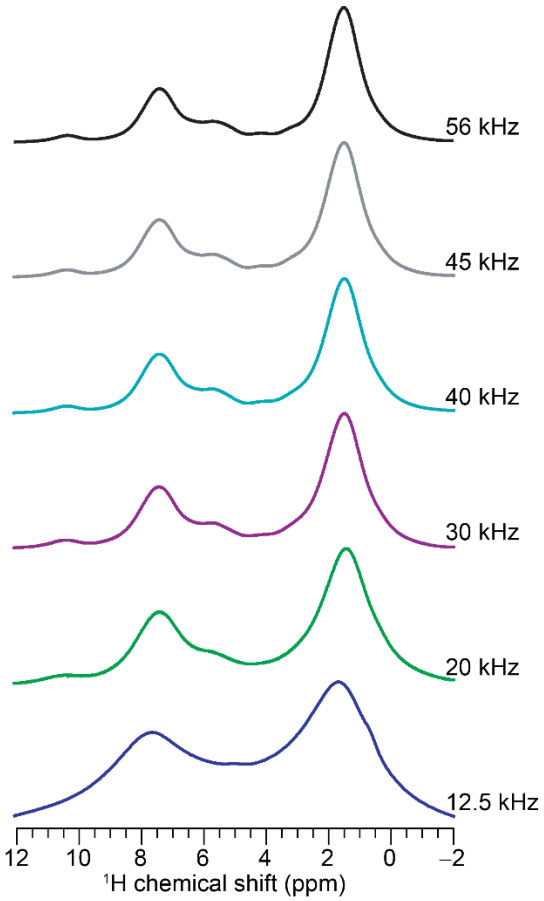

Figure S10. Solid-state 1D ^{1}H MAS NMR spectra of solid **PBI-1** aggregates acquired at 18.8 T (800.1 MHz) with variable MAS frequency, as indicated alongside the spectra.

For homogeneously broadened ^{1}H NMR spectra, the signals tend to narrow down upon increasing MAS rate due to the averaging of dipolar interactions. However, in the case of inhomogeneous broadening caused by different **PBI-1** aggregates with different domain sizes, the resolution does not improve much as the MAS frequency is increased. Signal broadening at MAS rates of 10-12 kHz compared to 4 kHz MAS is expected to originate from the sedimentation or large domain aggregation caused by the mechanical (centrifugal) force experienced by the sample inside the rotor. This line broadening as a function of MAS rates in the range of 4-12 kHz is reversible. We believe that the broader signals upon increasing MAS to 10-12 kHz are due to the deposition of **PBI-1** solid aggregates on the inner walls of the rotor (as seen in conventional centrifugation techniques), and more solution-like **PBI-1** aggregates remain at the central part of the cylindrical rotor, where it experiences a relatively lower

mechanical force. At lower MAS frequencies of 4 kHz or below, the **PBI-1** aggregates resemble a more uniform "slurry-like" mixture.

Table S5. 1D ^{1}H HR-MAS NMR linewidths of **PBI-1** aggregates-$CDCl_3$ (22:78) mixture at different MAS frequencies.

PBI-1:$CDCl_3$ (22:78) MAS (kHz)	FWHM (Hz)	
	7.3 ppm	8.2 ppm
4	264	300
6	290	325
8	330	348
10	380	400
12	450	432

10. References

1. I. Schnell, A. Lupulescu, S. Hafner, D. E. Demco, H. W. Spiess, *J. Magn. Res.* 133, 61-69 (1998).
2. S. Samanta, D. Chaudhuri, *J. Phys. Chem. Lett.* 8, 3427 (2017).
3. H. M. M. ten Eikelder, A. J. Markvoort, T. F. A. de Greef, P. A. J. Hilbers, *J. Phys. Chem. B* 116, 5291-5301 (2012).
4. Gaussian 16, Revision C.01, M. J. Frisch, G. W. Trucks, H. B. Schlegel, G. E. Scuseria, M. A. Robb, J. R. Cheeseman, G. Scalmani, V. Barone, G. A. Petersson, H. Nakatsuji, X. Li, M. Caricato, A. V. Marenich, J. Bloino, B. G. Janesko, R. Gomperts, B. Mennucci, H. P. Hratchian, J. V. Ortiz, A. F. Izmaylov, J. L. Sonnenberg, D. Williams-Young, F. Ding, F. Lipparini, F. Egidi, J. Goings, B. Peng, A. Petrone, T. Henderson, D. Ranasinghe, V. G. Zakrzewski, J. Gao, N. Rega, G. Zheng, W. Liang, M. Hada, M. Ehara, K. Toyota, R. Fukuda, J. Hasegawa, M. Ishida, T. Nakajima, Y. Honda, O. Kitao, H. Nakai, T. Vreven, K. Throssell, J. A. Montgomery Jr., J. E. Peralta, F. Ogliaro, M. J. Bearpark, J. J. Heyd, E. N. Brothers, K. N. Kudin, V. N. Staroverov, T. A. Keith, R. Kobayashi, J. Normand, K. Raghavachari, A. P. Rendell, J. C. Burant, S. S. Iyengar, J. Tomasi, M. Cossi, J. M. Millam, M. Klene, C. Adamo, R. Cammi, J. W. Ochterski, R. L. Martin, K. Morokuma, O. Farkas, J. B. Foresman, D. J. Fox, Gaussian, Inc., Wallingford CT, **2016**.
5. (a) R. K. Harris, P. Hodgkinson, V. Zorin, J. N. Dumez, B. Elena-Hermann, L. Emsley, E. Salager, R. S. Stein, *Magn. Reson. Chem.* 48, S103-S112 (2010). (b) G. N. M. Reddy, D. S. Cook, D. Iuga, R. I. Walton, A. Marsh, S. P. Brown, *Solid State Nucl. Magn. Reson.* 65, 41-48 (2015).
6. P. A. Korevaar, C. Schaefer, T. F. A. de Greef, E. W. Meijer, *J. Am. Chem. Soc.* 134, 13482-13491 (2012).